CARBON 73 (2014) 78–86

Available at www.sciencedirect.com

ScienceDirect

journal homepage: www.elsevier.com/locate/carbon

Annealing-induced structural changes of carbon onions: High-resolution transmission electron microscopy and Raman studies

Kirill Bogdanov [a], Anatoly Fedorov [a], Vladimir Osipov [b], Toshiaki Enoki [c], Kazuyuki Takai [c,d], Takuya Hayashi [e], Victor Ermakov [f], Stanislav Moshkalev [f], Alexander Baranov [a,*]

[a] Saint Petersburg National Research University of Information Technologies, Mechanics and Optics, Saint Petersburg 197101, Russia
[b] Ioffe Physical-Technical Institute, Saint Petersburg 194021, Russia
[c] Department of Chemistry, Tokyo Institute of Technology, 2-12-1, Ookayama, Meguro-ku, Tokyo 152-8551, Japan
[d] Department of Chemical Science and Technology, Hosei University, 3-7-2, Kajino, Koganei, Tokyo 184-8584, Japan
[e] Faculty of Engineering, Shinshu University, 4-17-1 Wakasato, Nagano 380-8553, Japan
[f] Center for Semiconductor Components, State University of Campinas, Campinas, Brazil

ARTICLE INFO

Article history:
Received 22 November 2013
Accepted 13 February 2014
Available online 18 February 2014

ABSTRACT

The first- and second-order Raman spectra of carbon nano-onions (CNOs), produced via annealing of detonation nanodiamonds with a mean grain size of ~5 nm in the argon ambience at the maximal temperature of annealing process (T_{MAX}) varying from 1500 to 2150 °C, are analyzed together with the high-resolution transmission electron microscopy (HRTEM) images. The combined analysis provides a deep insight into the annealing-induced atomic-scale structural modifications of the CNO nanoparticles. The Raman and HRTEM data unambiguously demonstrate the reduction in the number of defects in the CNO structure, as well as indicate the conversion from the diamond sp^3-bonded carbon phase to the sp^2-bonded carbon phase with increasing T_{MAX} and its almost full completion for T_{MAX} = 1600 °C.

1. Introduction

Multilayered quasi-spherical carbon nanoparticles, or carbon nano-onions (CNOs), currently attract much attention because of their unique structural and physical properties, which are different from the properties of the other nano-sized carbon materials—including nanodiamonds, graphene, fullerenes, and carbon nanotubes [1–11]. The structure of this material is still under discussion and usually described as a few enclosed fullerene-like layers or concentric graphitic shells, with a hollow inside, nanodiamond core or perfect fullerene in the centre [1]. CNOs have been considered as potentially interesting material for a number of applications. As a solid lubricant, CNOs can provide better lubrication than the commonly used graphitic materials [2]. Perfect shielding capabilities of CNOs at microwave, infrared and terahertz frequencies have also been demonstrated recently [3–5]. Besides being used as an electrode material for Li-ion batteries, CNOs

* Corresponding author.
E-mail address: a_v_baranov@yahoo.com (A. Baranov).
http://dx.doi.org/10.1016/j.carbon.2014.02.041
0008-6223/

were used as electrode materials for supercapacitors due to their large external surface area, which is easily accessible for alkali ion adsorption [6]. CNOs also find applications in fuel cells [7], heterogeneous catalysis [8], gas and energy storage [9] and electro-optics [10]. Finally, hollow CNOs are promising biocompatible nanocapsules for drug delivery systems [11].

Among various methods used for the production of CNOs, the annealing of 4–5-nm detonation nanodiamonds in the inert atmosphere is one of the most common [12]. The primary CNO particles obtained with this method consist of very defective concentric carbon sp^2 shells enclosed one into another. However, the number and types of defects can be essentially reduced via ordering the CNO structure by increasing the maximal annealing temperature T_{MAX} [1,13,14]. Since the atomic-scale structure of CNOs is a key parameter determining their mechanical, electronic and electromagnetic properties, the possibility to control the annealing-induced structural transformation is critically important for the fabrication of the CNO-based materials with desired functional properties.

A first comprehensive study of the annealing-induced structural transformation in CNOs has been done using the X-ray diffraction (XRD) technique about one decade ago [15]. Unfortunately, the XRD did not allow getting a reliable data on the CNO structural changes with increasing T_{MAX} above 1700 °C. For example, the changes in the coherent scattering sizes of graphitic nanocrystals did not exceed ~8% in the T_{MAX} range of 1700–2000 °C. Therefore, other independent precise methods are needed to detect the fine changes in the structure of CNOs during their transformation with annealing procedure.

The Raman scattering, which is one of the most powerful methods of studying graphitic materials, is a quite adequate technique for this purpose. This method provides a contactless and rapid way of getting information on chemical composition, structural properties and morphology of different carbon allotropes—including nanostructures like graphene, nanodiamonds, fullerenes and nanotubes [13,16–24]. The Raman spectroscopy has already been used for studying the CNO structures and, particularly, the annealing-induced structural transformation in CNOs synthesized from detonation nanodiamonds [1,14,24–26]. However, important aspects of the temperature-induced CNO structural changes are still not clear enough due to the difficulties in getting their Raman spectra of good quality.

In this work, we apply a new Raman technique (StreamLine™ Plus, Renishaw), which allows measuring the excellent quality Raman spectra of highly absorbing CNO samples (without damaging the samples) by using high laser power with reduced laser power density. We analyze the first- and second-order Raman spectra of CNOs, produced by annealing of detonation nanodiamonds with grain size of ~5 nm in the argon atmosphere at T_{MAX} varying from 1500 to 2150 °C, to understand the annealing-induced atomic-scale structural modifications of the CNO nanoparticles. The Raman data evidences a reduction in the number of defects in the CNO structure, points to its conversion from sp^3 to sp^2 phase, and shows the transformation of the CNO shape from quasi-spherical to polyhedral, probably faceted, with increasing T_{MAX}.

2. Materials and methods

CNOs were prepared via annealing of the well-purified nanodiamond powder (grain size ~5 nm, ash content <0.03 wt.%) in a large-scale, high-temperature commercial furnace SCC-U-80/150 (manufactured by Kurata Giken Co. Ltd., Aichi, Japan) in the dry argon atmosphere, along with the heating process with T_{MAX} of up to 1500–2150 °C, similar to the method described in Ref. [27]. Here we used the chemically superpurified detonation nanodiamonds, which were practically free (<14 ppm for each item) from the 3*d*-transition metal impurities like Fe and Ni, in order to exclude their parasitic catalytic impact on the possible particle growth and enlargement during the heat treatment process. The argon gas, filling the closed internal volume of the electrical furnace after its preliminary evacuation up to the technical vacuum, was under the pressure of ~50 kPa at 300 K. The gas pressure was kept fixed inside the furnace during the annealing, until the furnace was cooled down to the room temperature.

The annealing procedure was performed as follows: the nanodiamond powder in a graphite crucible was heated from the initial temperature of 950 °C up to the desired maximal temperature T_{MAX} in the range of 1500–2150 °C, with a heating rate of about 15 °C per minute, kept at this temperature for 20 min, and then cooled down to the room temperature, with a cooling rate of about 0.7–1.0 °C per second during the first 300 °C interval of cooling. The temperature of the crucible with the sample inside was controlled by optical pyrometer (Chino Corporation AL3000/AH3000) with accuracy of about 1% in the range 1500–2100 °C. Seven CNO samples were thus prepared for the study, with T_{MAX} of 1500, 1550, 1600, 1650, 1750, 1950, and 2150 °C.

The high resolution transmission electron microscope (HRTEM) JEOL JEM 2010FEF, 200 kV was used for the observation of the annealing-induced modification of the samples' structure. A relatively low acceleration voltage of about 120 kV was intentionally chosen to prevent a destruction of the internal and external structure of the nanoparticles and graphene sheets during their prolonged exposure to the focused electron beam. The actual lateral resolution was high enough to resolve the internal structure of the isolated CNO nanoparticles.

The Raman spectra of the CNO samples were measured using "inVia" Renishaw micro-Raman spectrometer with the 457.9- and 514.5-nm lines of the Ar^+ laser and the 633-nm line of the He–Ne laser as the excitation sources. The spectra were collected in the backscattering geometry using the 50× Leica objective (NA = 0.78), and normalized on a spectral sensitivity of the "inVia" Renishaw measured with a black-body radiation unit. The laser power of 20 W/cm^2 on the sample surface was used, preventing the sample heating. The samples for the Raman measurements were prepared by depositing and drying a drop of the aqueous colloid dispersion of the CNO powder on a copper substrate.

3. Results and discussion

3.1. HRTEM analysis

The representative images of different regions of the CNO samples annealed at T_{MAX} of 1500, 1650, and 2150 °C are presented in Fig. 1. They show that CNO particles have mean size ca. 6 nm and are very defective in comparison with the ideal graphene sheet structure, even though it gradually becomes less defective with increasing T_{MAX}. The CNOs have closed quasi-spherical or polyhedral-like shape, with the aspect ratio between ~1:1 and ~2:1, and consist of several (up to 7–10) graphene-like shells enclosed one into another. The outermost shells of the CNOs, which are especially defective, can be split and even exfoliated from the main core, and can have ripples or small loosely linked and fluttered fragments. Some isolated and loosely linked bended fragments with high local curvature appeared from the outermost shells of neighboring CNO nanoparticles are clearly seen in the HRTEM images in the figure (fragments *b*, *c*, *d*, *g*, *h*, *i*). Even the single isolated mono- or few-layer graphene strips of 10–20 nm in size, ideally flat or slightly folded, bended and twisted, can exist in the powder as a rare minority phase (see Fig. 1, fragments *b*, *d*, *f*, *g*). The averaged interlayer distance between the carbon shells varies between 0.35 and 0.42 nm for the majority of the CNO nanoparticles. The CNOs annealed at 1500 °C have the most dense onion-like structure, with the smallest interlayer distance and badly featured graphene facets but without a remarkable hollow structure (Fig. 1, fragments *a*, *b*, *c*). Some traces of the remaining cubic diamond cores can also be found in the material annealed at 1500 °C (Fig. 1, fragment *a*, see the lattice-fringe area with characteristic (1 1 1) interplanar spacing of 0.21 nm surrounded by the dotted circle).

The remaining diamond cores are present in the CNO powder due to the incomplete carbonization of the minor nanodiamond particles with sizes exceeding ~10–15 nm. Further annealing at the elevated temperature of 2150 °C leads to the appearance of less dense polyhedral particles, with a nanometer-size hollow interior and well-featured graphene facets, and the large-scale graphene sheets (Fig. 1, fragments *g*, *h*, *i*). The increase of T_{MAX} up to 2150 °C leads to the continuous formation of the flat graphene domains inside the CNO particles (Fig. 1, fragment *i*).

The presented HRTEM images clearly demonstrate a great morphological variety of local, on the nanometer scale, structures of the CNO samples, which complicate the classification of their structural peculiarities. In this case, the micro-Raman spectroscopy, providing a micrometer spatial resolution, is a

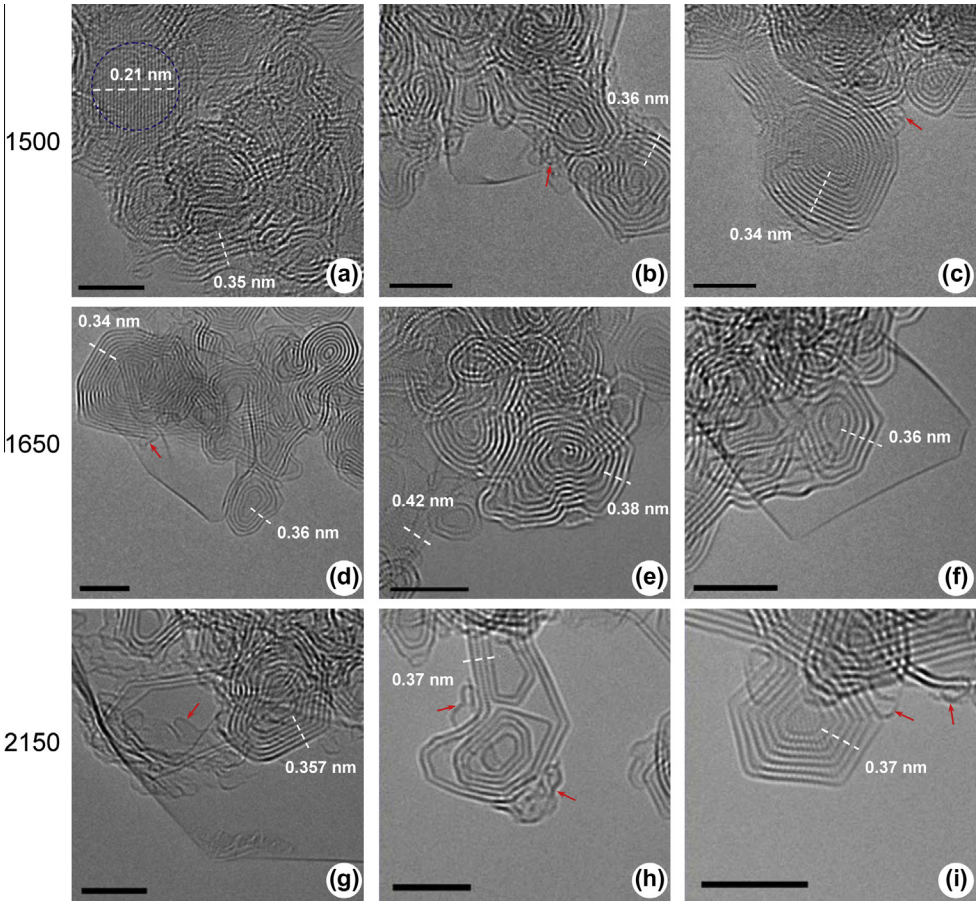

Fig. 1 – Representative HRTEM images of different regions of CNO samples annealed at temperatures T_{MAX} of (*a*, *b*, *c*) 1500 °C, (*d*, *e*, *f*) 1650 °C and (*g*, *h*, i) 2150 °C in the argon atmosphere. Small isolated and loosely linked bended graphitic sheets with high local curvature are marked by red arrows. Scale bars of 4 nm are shown. (A colour version of this figure can be viewed online.)

tool that can be used to get the integral structural information reflecting the dominant structural forms and the temperature-induced transformation of the CNO samples.

3.2. *Raman analysis*

In Fig. 2 we show the examples of the room-temperature first- and second-order Raman spectra of the CNO samples annealed in the argon atmosphere at T_{MAX} ranging from 1500 to 2150 °C. The spectra were excited at the 514.5-nm wavelength. The weak continuous backgrounds were subtracted. It was found that position, the intensity and linewidth of the *G* band (~1590 cm^{-1}) remained practically independent of the annealing temperature, so that all the spectra were normalized using the *G* band integral intensity.

The spectra are seen to be dominated by the *D* and *G* bands at 1343 and 1590 cm^{-1}, as well as by the *G'* band at 2704 cm^{-1}. The pronounced annealing-induced changes in the spectra are clearly seen in the width of the *D* band, Raman intensities near 1500 cm^{-1}, and the parameters of the *G'* band. The spectra also contain a few other Raman bands, characteristic for disordered graphite nanomaterials, whose parameters (positions, bandwidths, relative intensities and dispersion) reflect the origin of the bands, local structure of nanographites, as well as the presence and quantity of the local structural disorder [17–24].

To find the positions, bandwidths and intensities of the Raman peaks, the spectra were fitted with the Voigt line shapes using the WiRE™ 4 and Origin 8.5 inbuilt fitting procedures. A representative example of the fitting of the first- and second-order Raman spectra of the CNO nanoparticles annealed at T_{MAX} = 1650 °C and excited at 514.5 nm is shown in Fig. 3. The assignment of the Raman bands to the phonon modes of the CNOs and their overtones are shown by arrows. To avoid errors in the assignment, the positions and dispersions of the bands in the first- and second-order Raman spectra were analyzed in details. It was found that the spectra of all samples could be well fitted in such a way that the positions of all the second-order bands marked in Fig. 3b coincided (with a good accuracy) with the sum of the Raman shifts of the bands in the first-order spectrum, and their relative intensities correlated with those of the fundamental Raman bands. The observation of the combine tones of weak Raman bands and the strong *D* or *G* band proved the correctness of the weak bands positioning in the first-order spectra and indicated their origin in the vibration subsystem of the CNOs. The dispersions of the most overtones (combined tones) were obtained using the 457.9-, 514.5-, and 633-nm excitation wavelengths (corresponding to the energies of 2.706, 2.408, and 1.958 eV) and compared with the dispersions of their first-order constituents, which served as additional argument for the band assignment to the vibrational modes of the CNOs.

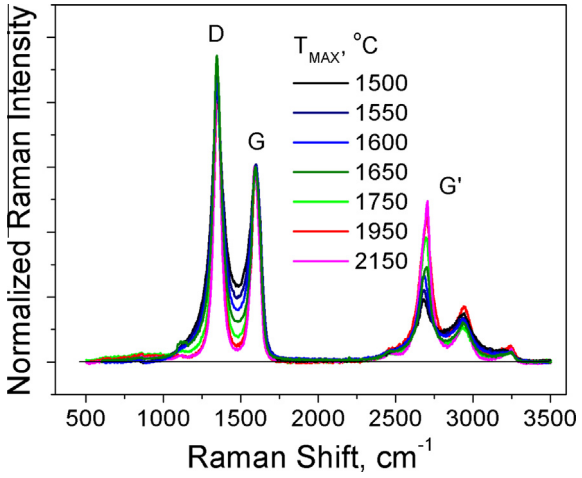

Fig. 2 – The first- and second-order Raman spectra of CNO nanoparticles annealed at different temperatures in the argon atmosphere. T_{MAX} are the peak annealing temperatures; excitation wavelength is 514.5 nm. (A colour version of this figure can be viewed online.)

The above analysis shows that the bands in the Raman spectra of CNOs can be unambiguously assigned to the well-known vibrational modes of disordered graphitic materials. The first-order spectrum shown in Fig. 3a consists of characteristic peaks centered at about 860 cm^{-1} (oTO), 1125 cm^{-1} (TPA), 1350 cm^{-1} (*D*), 1530 cm^{-1} (*A*), 1587 cm^{-1} (*G*), and 1625 cm^{-1} (*D'*), whereas in the second-order spectrum shown in Fig. 3b the overtones and combined tones of the peaks are resolved at 2470 cm^{-1} (TPA + *D*), 2695 cm^{-1} (*G'*), 2875 cm^{-1} (*D* + *A*), 2940 cm^{-1} (*D* + *G*), 3175 cm^{-1} (2*G*), and 3250 cm^{-1} (2*D'*). Here the wavenumbers of the bands are shown for the 514.5-nm excitation wavelength.

A small nondispersive peak at ~860 cm^{-1} can be assigned to the oTO-phonon mode near the Γ point of the Brillouin zone. This mode becomes active due to the graphene plane curvature [14,28]. The 1125-cm^{-1} peak shows positive dispersion, which is a fingerprint of the transpolyacetylene-(TPA)-like structures. Following Ferrari [29], we suggest that the TPA-like chains are formed at the zigzag edges of the defective CNO shells. The 1125-cm^{-1} band can then be assigned to a local vibration mode of the TPA-like chains, which is weakly coupled to other phonon modes of the CNO particle. The assignment is supported by the presence of the dispersive combined tone (TPA + *D*) at 2470 cm^{-1} in the Raman spectra of the CNOs. The observed positive dispersion of this band proves the correctness of the assignment, since the alternative assignment of the 2450-cm^{-1} band to the combined tone iTO + LA, proposed for the second-order Raman spectrum of graphene monolayer in Ref. [30], implies a negative band dispersion. The TPA band intensity is assumed to be proportional to the number of the zig-zag chains in the CNO shells.

The *G* band in the Raman spectra of carbon materials indicates the presence of the graphitic sp^2 phase and corresponds to the E_{2g} phonon mode (iTO and LO) at the Brillouin zone center (the in-plane bond stretching of the sp^2-bonded C atoms in hexagonal rings), i.e. to the two-dimensional graphene-like structure [17]. The position and FWHM of the *G* band are considered as a measure of the disorder present in the form of distorted hexagonal rings and chains. The higher the disorder in the structure, the lower the Raman shift of the *G* band and the larger its bandwidth [17,18].

The *D* band indicates the breathing mode of the sixfold aromatic rings in carbon network and is assigned to the phonons of A_{1g} symmetry at the K point of the Brillouin zone.

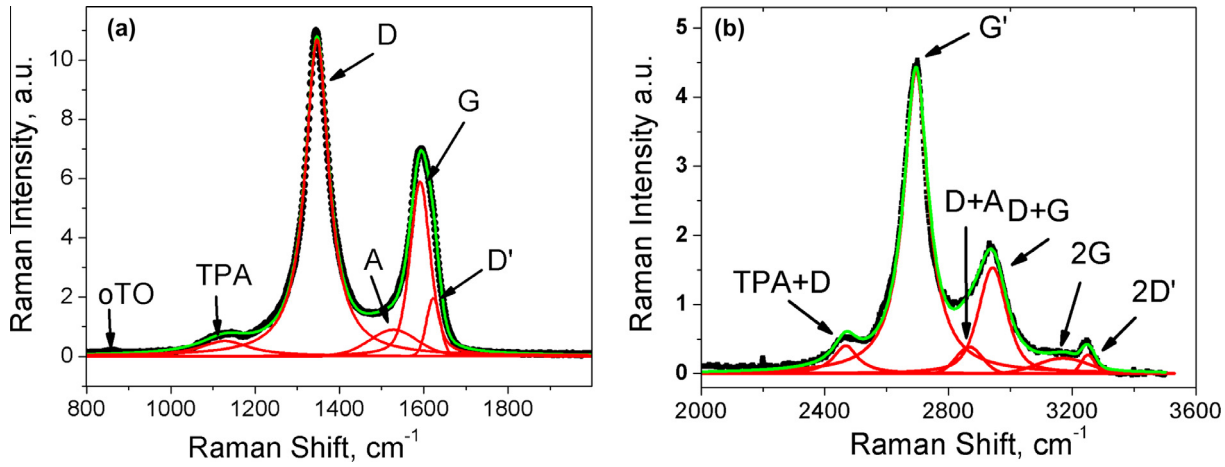

Fig. 3 – (a) and (b) are the representative examples of deconvolution of the first- and second-order Raman spectra of CNO nanoparticles annealed at 1650 °C. The spectra are excited at 514.5 nm. (A colour version of this figure can be viewed online.)

[25,31–33]. This mode becomes active in the first-order Raman scattering due to the relaxation of the momentum conservation in presence of the structural disorder of the graphite 2D layers, which most likely occurs in the presence of armchair edges of the carbon network [16,20,34–36]. The growth in the *D* band intensity with the structural disorder is widely used to quantify the disorder. Note that the armchair and zigzag edges are always present at the graphite-nanocrystal boundaries and carbon-network discontinuities, and can be considered as structural disorder. The *D* band integral intensity in this situation is expected to be proportional to the number of edges and/or discontinuities of the hexagonal carbon network of the CNO shells.

The broad dispersionless *A* band at about 1530 cm^{-1} is usually assigned to the amorphous carbon [37], which exists, for instance, in the form of interstitial disordered carbons with the sp^3 links outside or inside the planes of the aromatic rings [38,39]. The relative intensity of the *A* band can be used in this case as a parameter for the sp^3 content [40]. On the other hand, the presence of the five- and seven-membered carbon rings or complex assembled clusters on their base in the sample can also allow for the existence of the *A* band [41,42]. A presence of the five- and seven-membered carbon rings is expected in the regions of high local curvature of the CNOs shown in Fig. 1 by red arrows. In any case, its intensity relative to that of the *G* peak (I_{1530}/I_G) can serve as the indication of the relative content of the amorphous carbon in the disordered graphites [43]. The observation of the combined tone *D*+*A* in the Raman spectra indicates that the vibration subsystems of the sixfold aromatic rings of the CNO shells and the "amorphous" structures are coupled. This fact supports the presence of the amorphous carbons inside the planes of the aromatic rings.

We analyzed the temperature-induced changes of the above-mentioned parameters of the characteristic lines in the Raman spectra, which reflect the structural modification of the CNO samples.

The position of *G*-band (about 1590 cm^{-1}) in the studied CNOs does not change noticeably with T_{MAX}, and is close to that in non-disordered graphene [19] even for T_{MAX} = 1500 °C, where CNOs are disordered as evidenced by HRTEM and Raman (*D*-band, *A*-band, and oTO mode) results. The *G*-band position is often considered as a measure of the disorder present in the form of distorted hexagonal rings and chains [17,18]. However, it depends not only on the structural distortion but also on the position of the Fermi level. Indeed, the *G*-band exhibits a blue shift as the Fermi level deviates from the Dirac point even in non-disordered graphene [44]. The compensation of these contributions is most likely responsible for the observed invariant *G*-band position irrespective of the structural change accompanied by the increase of T_{MAX}, which will be discussed below with respect to the *G'* band.

Fig. 4 shows the T_{MAX} dependencies of the normalized integrated intensity (4a) and width (4b) of the *D* band, and the normalized integrated intensities of the TPA band (4c), *D'* band (4d), A band (4e), and *G'* band (4f) observed in the spectra excited at 514.5 nm. Analogous dependencies were found for the 457.9 and 633 nm excitations.

In contrast to the case of the *G* band, the twofold decrease of the I_D/I_G ratio (Fig. 4(a)), along with the decrease of the *D* band width from 85 to 58 cm^{-1} (Fig. 4(b)), was observed when T_{MAX} was increased from 1500 to 2150 °C, indicating significant changes in the edge structures of the studied CNOs. The reduction in the number of discontinuities in the CNO hexagonal carbon shells containing the armchair edges is most likely responsible for the observed changes in the Raman spectra. As for the zigzag chains at the CNO shell edges, an almost fourfold reduction of the normalized TPA band intensity I_{TPA}/I_G with T_{MAX}, shown in Fig. 4(c), indicates a simultaneous decrease in the number of defects such as the zigzag chains. This conclusion is supported by a similar T_{MAX} dependency of the *D'*-band intensity $I_{D'}/I_G$, which is plotted in Fig. 4(d). Indeed, the *D'* band is also related to the electronic process of scattering at the zigzag sites, and it is natural to expect a decreasing of its intensity with the number of zigzag chains (analogous to the decreasing of the TPA-band intensity).

A more than ten times decrease of the *A*-band intensity (Fig. 4(e)) is the most prominent feature of the temperature-induced changes in the CNO Raman spectra, showing a strong reduction of the amorphous carbon phase in the CNO

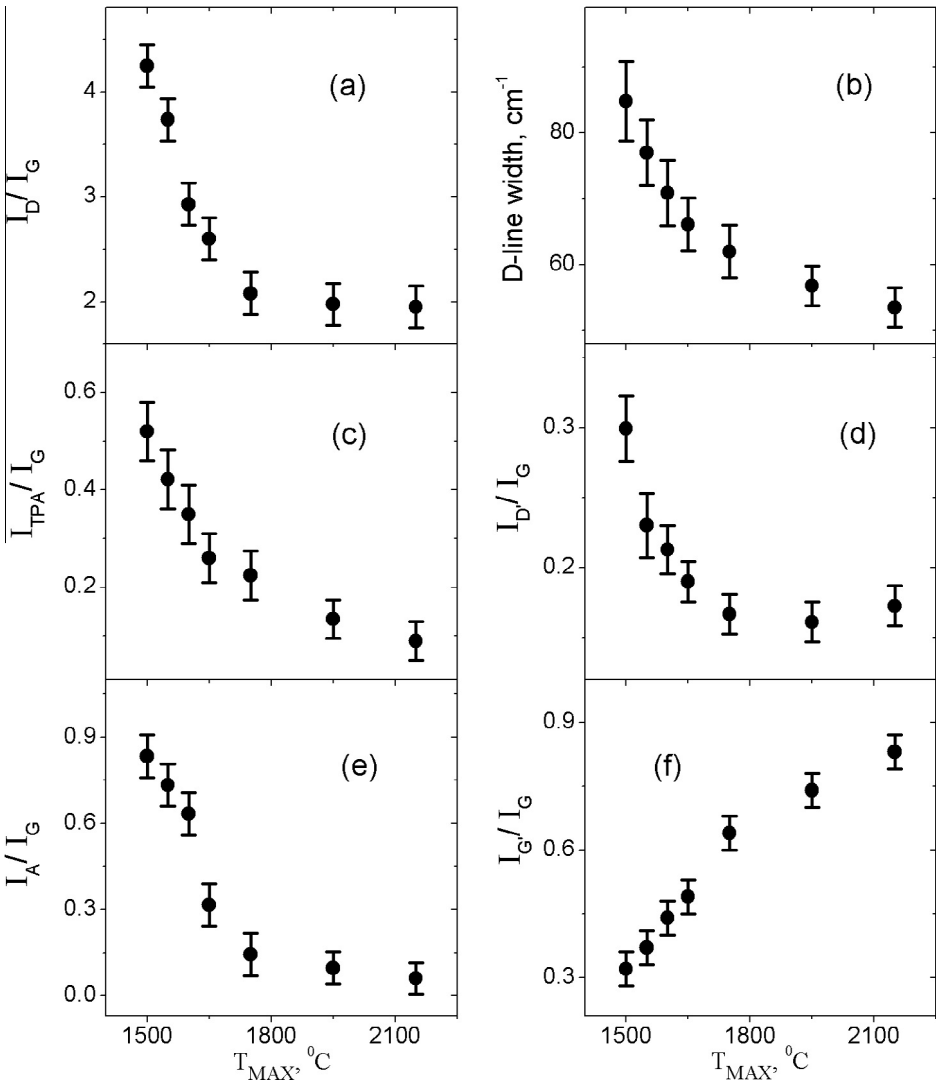

Fig. 4 – Temperature-induced changes of important parameters of the characteristic bands in the Raman spectra, reflecting the structural modification of the CNOs. (a) and (b) are the integrated intensity ratio (I_D/I_G) and linewidth of the *D* band; (c), (d), (e), and (f) are the integrated intensity ratios of the TPA band (I_{TPA}/I_G), *D'* band ($I_{D'}/I_G$), *A* band (I_A/I_G), and *G'* band ($I_{G'}/I_G$). The spectra are excited at 514.5 nm.

samples with the heat treatment. It should be noted that the intensity of the combined tone band *D*+*A* reduced only by a factor of three. This fact shows that there is probably some amount of the amorphous carbon phase outside the hexagonal carbon shells, which contributes only to the *A*-band intensity and almost completely disappears upon the annealing.

Another two prominent changes in the CNO Raman spectra are the increase of the *G'*-band integral intensity and appearance of the *G'*-band doublet structure with T_{MAX}. As can be seen from Fig. 4(f), an almost threefold rise of the normalized *G'*-band intensity ($I_{G'}/I_G$) was observed with increasing T_{MAX} in the range 1500–2150 °C.

The general feature inherent to all dependencies presented in Fig. 4 is the saturation of the parameters of the Raman bands with the annealing temperature. This fact indicates the slowdown, and even the completion, of the temperature-induced structural changes of CNOs produced by the annealing of the superpurified detonation nanodiamonds, which are practically free from the transition 3*d*-metal catalytic impurities. The change in the *A*-band intensity is the most prominent one in the spectra. The intensity of the *A* band significantly reduces with T_{MAX} and eventually becomes negligible at the highest T_{MAX}. The sensitive change of the *A*-band intensity indicates that it is an appropriate parameter to characterize the structural changes of CNOs caused by the increase in T_{MAX}. The presence of the *A* band in the Raman spectra is related to the contribution of the residue sp^3 structure in the nanocarbon material. The observed remarkable change in the *A*-band intensity can be attributed to the conversion of the nanodiamond particles to the sp^2-carbon structure. It should also be noted that the *A*-band intensity, which is most sensitive to the change in the structure of the CNOs, rapidly decreases around 1600 °C, which is not that evident for other parameters of the Raman spectrum. This indicates that the conversion from the nanodiamond to sp^2 structure (carbonization) is almost completed around this temperature,

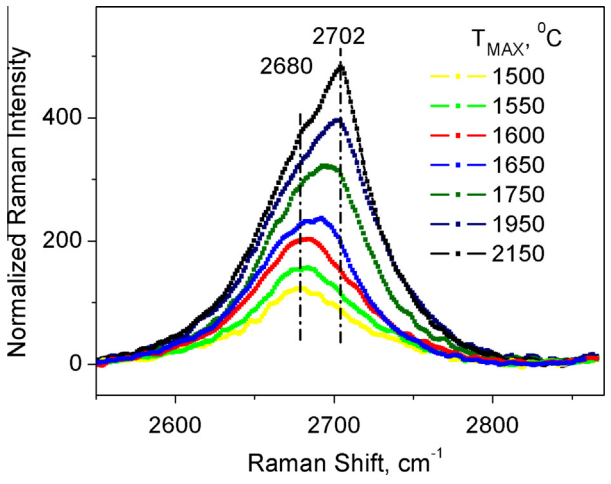

Fig. 5 – Appearance of doublet structure of G' band in Raman spectrum of CNOs with annealing temperature T_{MAX}. The spectra are normalized on the G-band integrated intensity. Excitation wavelength is 514.5 nm. Temperatures in °C and wavenumbers of the band are shown. (A colour version of this figure can be viewed online.)

and the structural change occurred with further annealing is mainly due to the development of the graphene-sheet-like structure. This conclusion is consistent with the observed imperfectness of the carbonization of the CNOs at T_{MAX} of 1500 °C, as well as with the HRTEM images showing the well-developed graphene-sheet structures in the CNOs prepared with T_{MAX} above 1600 °C.

Additional data on the stacking order of the hexagonal carbon network shells along the *c* axis (radius of CNOs) can be obtained from the temperature-induced modification of the *G'*-band shape shown in Fig. 5.

It is seen that the spectrum shape changes from a single Lorentzian-like band, typical for a single graphene layer and turbostratic nanographites without any stacking along the *c* axis, to a more complex Raman line structure, which is characteristic for multilayer ($N > 4$) graphene [23] and three-dimensional graphite. A similar annealing-induced transformation of the Raman spectra in the ~2700-cm^{-1} region has been reported for HOPG in Ref. [20], and explained by the increase in the stacking order of graphene layers along the *c* axis. In reference to our samples, the change in the shape of their spectra reflects the formation (at sufficiently high annealing temperatures) of the carbon structures consisting of nearly stacked graphene layers and faceted polyhedral CNOs, shown in Fig. 1*g–i* for the sample annealed at 2150 °C. This conclusion is in agreement with the data reported earlier for the spherical and polyhedral CNOs prepared from diamond nanoparticles [24].

The behavior of the *G'*-band to *G*-band intensity ratio, which is frequently used for the evaluation of the stacking order in graphene sheets, is more complicated. Meanwhile, this ratio is a more quantitative parameter than the change in the shape of the *G'* band. The value of the ratio does not depend solely on the stacking order of graphene sheets, but is also a function of the Fermi level energy. Indeed, it decreases with both the improvement of the stacking order of a graphene sheet and the deviation of the Fermi level from the Dirac point, where the ratio peaks [44]. The dependency of $I_{G'}/I_G$ on T_{MAX}, shown in Fig. 4(f), has a trend that is opposite to that of the structural ordering along the *c* axis as a function of T_{MAX}. This can be explained by the shift of the Fermi level. In the oxygen or ambient atmosphere, the Fermi energy of the carbon material with a graphene-like structure can be significantly downshifted by the charge transfer to the electrically negative oxygen-containing species attached to the sample [45,46]. The structures of CNOs with lower T_{MAX} have more defects acting as effective adsorption sites for oxygen-containing species and molecular oxygen, resulting in the lower energy of the Fermi level with respect to the Dirac point. As the structural ordering of the graphene sheet is improved with increasing T_{MAX}, the amount of the adsorbed or chemically bonded oxygen-containing species becomes smaller. Thus, the Fermi level of CNOs with higher T_{MAX} shifts toward the Dirac point. Then the observed change of the *G'*-peak intensity [show in Fig. 4(f)] is mainly caused by the change of the Fermi energy of CNOs following the elevation of T_{MAX}. This is also consistent with the observed insensitivity of the *G*-band position to the structural changes of CNOs with increasing T_{MAX}, where influence of the distortion of graphene-like sheets is compensated by that of shifting in the Fermi level toward the Dirac point.

4. Conclusion

The structural changes of carbon nano-onions (CNOs), obtained via annealing the detonation nanodiamonds with grain size of ~5 nm, have been investigated using the Raman spectroscopy and HRTEM images. The evolution of the carbon phase conversion from the sp^3 to sp^2 structure with increasing of the maximum annealing temperature T_{MAX}, and its almost full completion near T_{MAX} = 1600 °C, was evidenced by the change in both the HRTEM images and *A*-band intensity in the Raman spectra. It was revealed that the gradual development of the graphene-like sheets and the order of their stacking in CNOs can be well characterized by the change in the parameters of the TPA, *D*, *G*, *D'*, and *G'* bands in the Raman spectra. The observed increase in the *G'*/*G* bands intensity ratio with T_{MAX} was explained by the up-shift of the Fermi energy due to the reduction in the number of the oxygen-containing species attached to CNOs, which accompanies the development of the ordered graphene-like sheet structures. In addition to that, HRTEM revealed that defects remain in the local structure of CNOs, especially in the outmost layers of CNOs even for highest T_{MAX} of 2150 °C.

Acknowledgments

This work was supported by the Government of Russian Federation (Grant 074-U01), the Ministry of Education and Science of the Russian Federation (Projects 14.B25.31.0002), the Japan-Russia Research Cooperative Program within the grants RFBR 12-02-92107 ЯФ_а and JSPS, and the Grant-in-aid for Scientific Research No. 25410088 from JSPS. The authors thank Prof. Eiichi Yasuda of Tokyo Institute of Technology for his help with the use of electrical furnace of NEDO Nanofiber Project.

REFERENCES

[1] Kuznetsov VL, Butenko YuV. Nanodiamond graphitization and properties of onion-like carbon. In: Gruen DM, Shenderova OA, Vul' AYa, editors. Synthesis, properties and applications of ultrananocrystalline diamond, vol. 192. Dordrecht: Springer; 2005. p. 199–216.

[2] Street KW, Marchetti M, Vander Wal RL, Tomasek AJ. Evaluation of the tribological behavior of nano-onions in Krytox 143AB. Tribol. Lett. 2004;16:143–9.

[3] Maksimenko SA, Rodionova VN, Slepyan GYa, Karpovich VA, Shenderova O, Walsh J, et al. Attenuation of electromagnetic waves in onion-like carbon composites. Diam Relat Mater 2007;16(4):1231–5.

[4] Shenderova O, Grishko V, Cunningham G, Mossenkov S, McGuire G, Kuznetsov V. Onion-like carbon for terahertz electromagnetic shielding. Diam Relat Mater 2008;17(4–5):462–6.

[5] Kuzhir PP, Bychanok DS, Maksimenko SA, Gusinski AV, Ruhavets OV, Kuznetsov VL, et al. Onion-like carbon based polymer composite films in microwaves. Solid State Sci 2009;11(10):1762–7.

[6] Pech D, Brunet M, Durou H, Huang P, Mochalin V, Gogotsi Yu, et al. Ultrahigh-power micrometre-sized supercapacitors based on onion-like carbon. Nat Nanotechnol 2010;5(9):651–4.

[7] Xu B, Yang X, Wang X, Guo J, Liu X. A novel catalyst support for DMFC: onion-like fullerenes. J Power Sources 2006;162(1):160–4.

[8] Keller N, Maksimova NI, Roddatis VV, Schur M, Mestl G, Butenko VYu, et al. The Catalytic use of onion-like carbon materials for styrene synthesis by oxidative dehydrogenation of ethylbenzene. Angew Chem Int Ed 2002;41(11):1885–8.

[9] Sano N, Wang H, Alexandrou I, Chhowalla M, Teo KBK, Amartunga GAJ, et al. Properties of carbon onions produced by an arc discharge in water. J Appl Phys 2002;92(5):2783.

[10] Koudoumas E, Kokkinaki O, Konstantaki M, Cours S, Korovin S, Detkov P, et al. Onion-like carbon and diamond nanoparticles for optical limiting. Chem Phys Lett 2002;357:336–40.

[11] Zhang XQ, Chen M, Lam R, Xu X, Osawa E, Ho D. Polymer-functionalized nanodiamond platforms as vehicles for gene delivery. ACS Nano 2009;3(9):2609–16.

[12] Kuznetsov VL, Chuvilin AL, Butenko YuV, Mal'kov IYu, Titov VM. Onion-like carbon from ultra-disperse diamond. Chem Phys Lett 1994;222(4):343–8.

[13] Okotrub AV, Bulusheva LG, Kuznetsov VL, Butenko YuV, Chuvilin AL, Heggie MI. X-ray emission studies of the valence band of nanodiamonds annealed at different temperatures. J Phys Chem A 2001;105:9781–7.

[14] Osipov VYu, Baranov AV, Ermakov VA, Makarova TL, Chungong LF, Shames AI, et al. Raman characterization and UV optical absorption studies of surface plasmon resonance in multishell nanographite. Diam Relat Mater 2011;20(2):205–9.

[15] Tomita S, Burian A, Dore JC, LeBolloch D, Fujii M, Hayashi S. Diamond nanoparticles to carbon onions transformation: X-ray diffraction studies. Carbon 2002;40:1469–74.

[16] Tuinstra F, Koenig JL. Raman spectrum of graphite. J Chem Phys 1970;53(3):1126–30.

[17] Ferrari AC, Robertson J. Raman spectroscopy of amorphous, nanostructured, diamond-like carbon, and nanodiamond. Philos Trans R Soc A: Phys Math Eng Sci 1824;2004(362):2477–512.

[18] Ferrari AC, Rodil SE, Robertson J. Interpretation of infrared and Raman spectra of amorphous carbon nitrides. Phys Rev B 2003;67:155306.

[19] Gupta A, Chen G, Joshi P, Tadigadapa S. Raman scattering from high-frequency phonons in supported n-graphene layer films. Nano Lett 2006;6(12):2667–73.

[20] Pimenta MA, Dresselhaus G, Dresselhaus MS, Cancado LG, Jorio A, Saito R. Studying disorder in graphite-based systems by Raman spectroscopy. Phys Chem Chem Phys 2007;9(11):1276–91.

[21] Ferrari AC. Raman spectroscopy of graphene and graphite: disorder, electron–phonon coupling, doping and nonadiabatic effects. Solid State Commun 2007;143(1–2):47–57.

[22] Reich S, Thomsen C. Raman spectroscopy of graphite. Philos Trans R Soc Lond A 2004;362:2271–88.

[23] Malard LM, Pimenta MA, Dresselhaus G, Dresselhaus MS. Raman spectroscopy in graphene. Phys Rep 2009;473(5–6):51–87.

[24] Obraztsova ED, Fujii M, Hayashi S, Kuznetsov VL, Butenko YuV, Chuvilin AL. Raman identification of Onion-like carbon. Carbon 1998;36(5–6):821–6.

[25] Ferrari AC, Robertson J. Interpretation of Raman spectra of disordered and amorphous carbon. Phys Rev B 2000;61(20):14095–107.

[26] Tomita S, Sakurai T, Ohta H, Fujii M, Hayashi S. Structure and electronic properties of carbon onions. J Chem Phys 2001;114(17):7477–82.

[27] Osipov VYu, Enoki T, Takai K, Takahara K, Endo M, Hayashi T. Magnetic and high resolution TEM studies of nanographite derived from nanodiamond. Carbon 2006;44(7):1225–34.

[28] Saito R, Jorio A, Souza Filho AG, Grueneis A, Pimenta MA, Dresselhaus G, et al. Dispersive Raman spectra observed in graphite and single wall carbon nanotubes. Phys B Condens Matter 2002;323(1–4):100–6.

[29] Ferrari AC, Robertson J. Origin of the 1150 cm^{-1} Raman mode in nanocrystalline diamond. Phys Rev B 2001;63(12):121405.

[30] Mafra DL, Samsonidze G, Malard LM, Elias DC, Brant JC, Plentz F, et al. Determination of LA and TO phonon dispersion relations of graphene near the Dirac point by double resonance Raman scattering. Phys Rev B 2007;76(23):233407.

[31] Nemanich RJ, Solin SA. First- and second-order Raman scattering from finite-size crystals of graphite. Phys Rev B 1979;20(2):392–401.

[32] Lespade P, Al-Jishi R, Dresselhaus MS. Model for Raman scattering from graphitized carbons. Carbon 1982;20(5):427–31.

[33] Ferrari AC, Robertson J. Resonant Raman spectroscopy of disordered, amorphous, and diamondlike carbon. Phys Rev B 2001;64(7):075414.

[34] Katagiri G, Ishida H, Ishitani A. Raman spectra of graphiti edge planes. Carbon 1988;26(4):565–71.

[35] Sasaki K, Tokura Y, Sogawa T. The origin of Raman D band: bonding and antibonding orbitals in graphene. Crystals 2013;3(1):120–40.

[36] Cancado LG, Jorio A, Martins Ferreira EH, Stavale F, et alAchete CA, Capaz RB. Quantifying defects in graphene via Raman spectroscopy at different excitation energies. Nano Lett 2011;11(8):3190–6.

[37] Ungár T, Gubicza J, Trichy G, Pantea C, Zerda TW. Size and shape of crystallites and internal stresses in carbon blacks. Compos A Appl Sci Manuf 2005;36(4):431–6.

[38] Cuesta A, Dhemelincourt P, Laureyns J, Martinez-Alonso A, Tascon JMD. Raman microprobe studies on carbon materials. Carbon 1994;32(8):1523–32.

[39] Jawhari T, Roid A, Casado J. Raman spectroscopic characterization of some commercially available carbon black materials. Carbon 1995;33(11):1561–5.

[40] Yoshikawa M, Katagiri G, Ishida H, Ishitani A. Raman spectra of diamondlike amorphous carbon films. J Appl Phys 1988;64(11):6464–8.
[41] Koskinen P, Malola S, Häkkinen H. Evidence for graphene edges beyond zigzag and armchair. Phys Rev B 2009;80(7):073401.
[42] Dallas TEJ. Structural phases of disordered carbon materials. A dissertation in physics submitted to the Graduate Faculty of Texas Tech University in Partial Fulfillment of the Requirements for the Degree of Doctor of Philosophy 1996.
[43] Zerda TW, Xu W, Yang H, Gerspacher M. The effects of heating and cooling rates on the structure of carbon black particles. Rubber Chem Technol 1998;71(1):26–37.
[44] Das A, Pisana S, Chekraborty B, Piscanec S, Saha SK, Waghmare UV, et al. Monitoring dopants by Raman scattering in an electrochemically top-gated graphene transistor. Nat Nanotechnol 2008;3:210–5.
[45] Sumanasekera GU, Chen G, Takai K, Joly J, Kobayashi N, Enoki T. Charge transfer and weak chemisorption of oxygen molecules in nanoporous carbon consisting of a disordered network of nanographene sheets. J Phys Condens Matter 2010;22(33):334208.
[46] Sato Y, Takai K, Enoki T. Electrically controlled adsorption of oxygen in bilayer graphene devices. Nano Lett 2011;11(8):3468–75.